Article

Nuclear moments of indium isotopes reveal abrupt change at magic number 82

https://doi.org/10.1038/s41586-022-04818-7

Received: 10 June 2021

Accepted: 28 April 2022

Published online: 13 July 2022

Check for updates

A. R. Vernon[1,2,3]✉, R. F. Garcia Ruiz[2,4]✉, T. Miyagi[5], C. L. Binnersley[1], J. Billowes[1], M. L. Bissell[1], J. Bonnard[6], T. E. Cocolios[3], J. Dobaczewski[6,7], G. J. Farooq-Smith[3], K. T. Flanagan[1,8], G. Georgiev[9], W. Gins[3,10], R. P. de Groote[3,10], R. Heinke[4,11], J. D. Holt[5,12], J. Hustings[3], Á. Koszorús[3], D. Leimbach[11,13,14], K. M. Lynch[4], G. Neyens[3,4], S. R. Stroberg[15], S. G. Wilkins[1,2], X. F. Yang[3,16] & D. T. Yordanov[4,9]

In spite of the high-density and strongly correlated nature of the atomic nucleus, experimental and theoretical evidence suggests that around particular 'magic' numbers of nucleons, nuclear properties are governed by a single unpaired nucleon[1,2]. A microscopic understanding of the extent of this behaviour and its evolution in neutron-rich nuclei remains an open question in nuclear physics[3–5]. The indium isotopes are considered a textbook example of this phenomenon[6], in which the constancy of their electromagnetic properties indicated that a single unpaired proton hole can provide the identity of a complex many-nucleon system[6,7]. Here we present precision laser spectroscopy measurements performed to investigate the validity of this simple single-particle picture. Observation of an abrupt change in the dipole moment at $N = 82$ indicates that, whereas the single-particle picture indeed dominates at neutron magic number $N = 82$ (refs. [2,8]), it does not for previously studied isotopes. To investigate the microscopic origin of these observations, our work provides a combined effort with developments in two complementary nuclear many-body methods: ab initio valence-space in-medium similarity renormalization group and density functional theory (DFT). We find that the inclusion of time-symmetry-breaking mean fields is essential for a correct description of nuclear magnetic properties, which were previously poorly constrained. These experimental and theoretical findings are key to understanding how seemingly simple single-particle phenomena naturally emerge from complex interactions among protons and neutrons.

The atomic nucleus is formed by strongly interacting nucleons (protons, Z, and neutrons, N), packed tightly into a volume around a trillion times smaller than that of atoms. Hence, describing the atomic nuclei and predicting their properties at extreme values of mass and charge are the main long-standing challenges for nuclear science. Similar to electrons in an atom, the nucleons (protons and neutrons) in the atomic nucleus occupy quantum 'shells'. Thus, nuclei with a single valence particle or hole around a nuclear closed shell provide important foundations for our understanding of the atomic nucleus. Their simpler structure vastly reduces the complexity of the quantum many-body problem, providing critical guidance for the development of nuclear theory.

Recent advances in our understanding of the strong interaction and the development of many-body methods, combined with escalation in computer power, have enabled theoretical descriptions of increasingly complex nuclei. Isotopes around the proton closed shell $Z = 50$, are now the frontier of ab initio calculations[9,10]. The properties of these nuclei can be described by complementary many-body methods such as configuration interaction methods[4] and nuclear DFT[11]. This has led to an increased focus on studying this region of the nuclear chart (around $Z = 50$, $N = 50, 82$) over the past decade[2,8,12–14].

Here we present measurements of two fundamental properties of indium isotopes using precision laser spectroscopy: the (spectroscopic) magnetic dipole moment, μ, and the electric quadrupole moment, Q. Measurements were performed for the neutron-rich In ($Z = 49$) isotopes, reaching up to ^{131}In, which possesses a magic number of $N = 82$ neutrons (see Methods for details). With a single-proton-hole configuration with respect to the well-established[2,8,14] proton closed

[1]School of Physics and Astronomy, The University of Manchester, Manchester, UK. [2]Massachusetts Institute of Technology, Cambridge, MA, USA. [3]Instituut voor Kern- en Stralingsfysica, KU Leuven, Leuven, Belgium. [4]Experimental Physics Department, CERN, Geneva, Switzerland. [5]TRIUMF, Vancouver, British Columbia, Canada. [6]Department of Physics, University of York, Heslington, York, UK. [7]Institute of Theoretical Physics, Faculty of Physics, University of Warsaw, Warsaw, Poland. [8]Photon Science Institute, The University of Manchester, Manchester, UK. [9]IJCLab, CNRS/IN2P3, Université Paris-Saclay, Orsay, France. [10]Department of Physics, University of Jyväskylä, Jyväskylä, Finland. [11]Institut für Physik, Johannes Gutenberg-Universität Mainz, Mainz, Germany. [12]Department of Physics, McGill University, Montréal, Québec, Canada. [13]Engineering Department, CERN, Geneva, Switzerland. [14]Department of Physics, University of Gothenburg, Gothenburg, Sweden. [15]Department of Physics, University of Washington, Seattle, WA, USA. [16]School of Physics and State Key Laboratory of Nuclear Physics and Technology, Peking University, Beijing, China. ✉e-mail: vernona@mit.edu; rgarciar@mit.edu

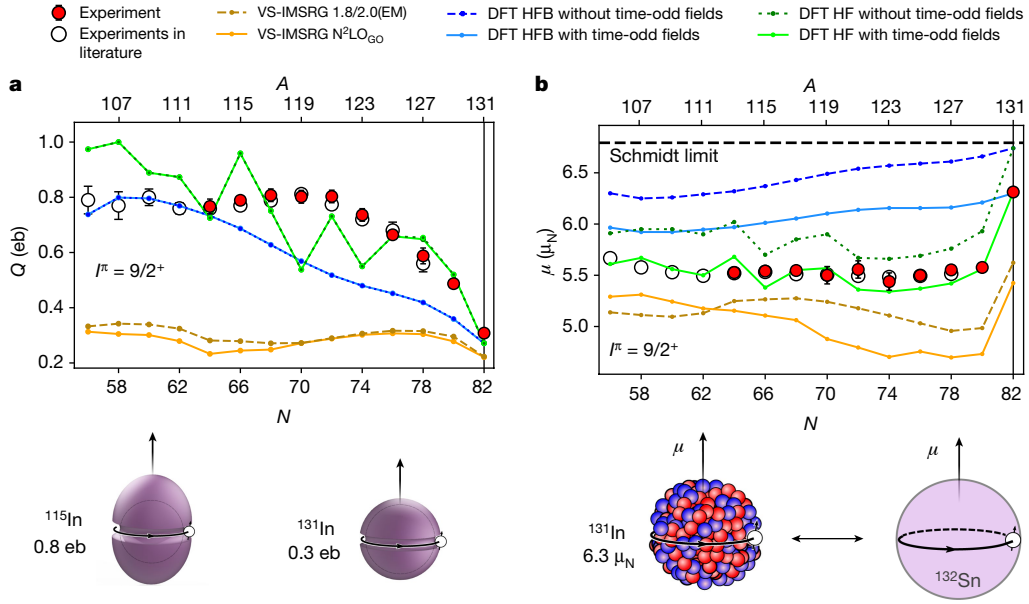

Fig. 1 | Evolution of nuclear electromagnetic properties for the $9/2^+$ ground states of $^{105-131}$In isotopes. a, **b**, The electric quadrupole moments (**a**) and magnetic dipole moments (**b**). The horizontal dotted line indicates the single-particle value (Schmidt limit). Experimental results are compared with theoretical calculations from ab initio VS-IMSRG and DFT. Literature experimental values for $^{105-127}$In were taken from ref. [7]. The evolution of collective properties of these isotopes is illustrated at the bottom of the figure: left, quadrupole polarization gradually reduces to a single-proton-hole value at $N = 82$; right, the magnetic dipole moments abruptly approach the value for a single proton hole in a ^{132}Sn core at $N = 82$, as the dominant effect changes from charge to spin distribution.

shell of $Z = 50$, the low-energy structure of the odd-mass indium isotopes is expected to be governed by a single-hole configuration in the proton orbit $\pi 1g_{9/2}$.

As we show here, the nuclear magnetic dipole moments of odd-mass indium isotopes are determined by the total spin distribution of the nucleus induced by the unpaired valence proton hole. This is schematically illustrated at the bottom right of Fig. 1. The nuclear electric quadrupole moment provides a complementary measurement of the nuclear charge distribution and is highly sensitive to the collective motion of all nucleons[15]. These observables together therefore explore distinct aspects of the nucleon distribution and measuring them across a large range of neutron numbers allows a unique insight into the evolution of the interplay between single-particle and collective nuclear phenomena.

Previously, the magnetic moments of the ground state $I^\pi = 9/2^+$ of indium isotopes were known to exhibit remarkably little variation over 22 isotopes, from $A = 105$ to 127 (see Fig. 1b open symbols)[7]. The constant value of the magnetic moment over such a long range of isotopes has been presented as an archetypal example of the independent-particle behaviour of single-particle states near a proton shell closure[6,7]. 'How do these seemingly simple patterns emerge from complex interactions among protons and neutrons?' and 'Do they prevail at extreme number of neutrons?' are two principal open questions that we address in this work.

In addition to the ground state, the indium isotopes can also exist in excited nuclear configurations with relatively long lifetimes—isomers—with spin $I^\pi = 1/2^-$. These isomeric states provide further insight and are expected to be described by a single-hole configuration based on a different proton orbital ($\pi 2p_{1/2}$). However, in contrast to the $I^\pi = 9/2^+$ states, the μ values of these isomeric states exhibit notable variations (see Fig. 3), posing a three-decades-long puzzle in our description of these nuclei[7].

To unravel the microscopic origin of the electromagnetic properties of these isotopes, we compare our experimental results with two complementary state-of-the-art theoretical methods: (1) ab initio valence-space in-medium similarity renormalization group (VS-IMSRG) calculations[9,16], which start from nucleon–nucleon interactions derived from chiral effective field theory[17], and (2) symmetry-breaking nuclear DFT[11,18]. The latter assumes nucleons moving within their own self-consistently generated spin-dependent broken-symmetry-confining potential. DFT provides a satisfactory description of bulk nuclear properties such as radii and binding energies across the whole nuclear chart[19–21]. Here we have developed its symmetry-restored version[22] to be able to provide accurate calculations of spectroscopic μ and Q moments.

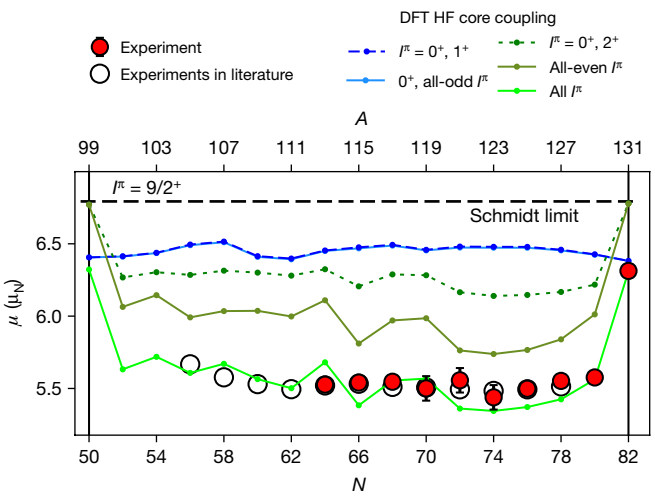

Fig. 2 | A breakdown of the contributions of the polarized core states. Breakdown of the contributions of the polarized core states to the final calculated μ values of the $I^\pi = 9/2^+$ state from the DFT HF calculations, compared with experiment. See text for details.

Experimental and theoretical developments

Our measurements were performed using the collinear resonance ionization spectroscopy (CRIS) technique at the ISOLDE facility of CERN[23] (see Methods for details). From the hyperfine structure, we

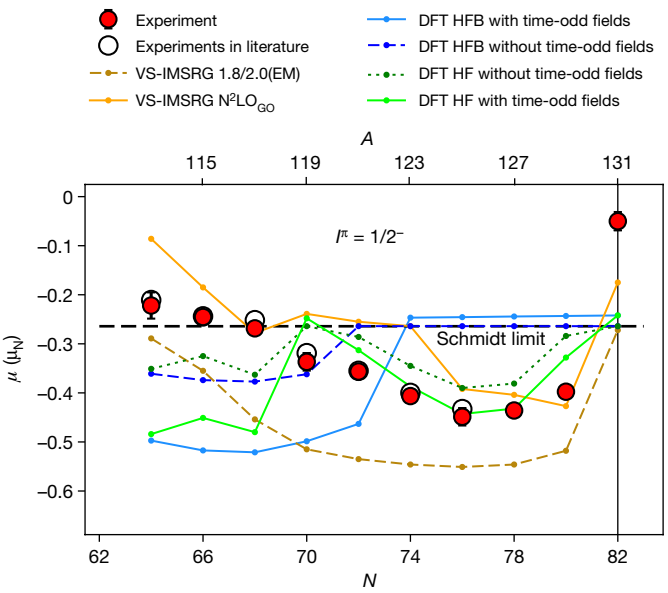

Fig. 3 | Nuclear magnetic moments for the 1/2⁻ isomeric states of $^{113-131}$In isotopes. Results are compared with ab initio and DFT calculations. The horizontal dotted line indicates the single-particle value (Schmidt limit). See text for more details.

extracted the magnetic dipole and electric quadrupole parameters A_{hf} and B_{hf} of the investigated atomic states, corresponding to the two long-lived nuclear states, $9/2^+$ and $1/2^-$, present in each isotope. Recent improvements in the sensitivity of the technique allowed us to achieve high-resolution spectroscopy measurements, despite production of the indium isotopes at rates below 1,000 atoms s^{-1} in the presence of large isobaric contamination. To enable these measurements, laser ionization spectroscopy schemes had to be developed that are both sensitive to low isotope rates from a large background and sensitive to nuclear properties through hyperfine structure, in addition to the development of increased accuracy atomic calculations for the extraction of their moments[24–26].

We performed ab initio VS-IMSRG calculations (see Methods for further details) using two different sets of initial two-nucleon (NN) and three-nucleon (3N) forces derived from chiral effective field theory[27,28]; the 1.8/2.0(EM)[17] and the more recent N^2LO_{GO} (ref. [29]). The 1.8/2.0(EM) set is constrained only by fitting to properties of two-nucleon, three-nucleon and four-nucleon systems. N^2LO_{GO} was recently developed to include Δ-isobar degrees of freedom and is also fit to reproduce saturation properties of infinite nuclear matter[29].

We performed DFT calculations using both Hartree–Fock (HF) and Hartree–Fock–Bogoliubov (HFB) approaches, corresponding to configurations of the nucleus constructed using single-nucleon (HF) or nucleon–hole pair excitations (HFB) as basis states, with HFB calculations introducing pairing correlations. The electromagnetic moments of semi-magic ± 1 nucleon systems, such as the indium isotopes, are well suited to study DFT time-symmetry-breaking (time-odd) contributions to the mean field[30,31], which vary with the time-reversal operator. These fields are predominantly generated by the two-body spin–spin interaction terms, and—up until now—were poorly constrained within DFT theory. However, they are of particular interest as our understanding of time-reversal-violating mean fields is critical to tackle open problems of modern physics, such as the search for new physics[32–34] and dark matter searches[35]. Our experimental results presented an excellent opportunity to perform and test these developments. To investigate the relative importance of time-odd fields and pairing correlations, DFT calculations were performed by turning 'on' and 'off' of each effect. See Methods for more details on the symmetry-restored calculations. Contrary to shell-model calculations based on empirical interactions, in which effective single-nucleon charges and g-factors are used to reproduce nuclear moments data, in our DFT and ab initio calculations, we use free single-nucleon g-factors and bare nucleon charges. In addition, the Landau parameter g'_0 was able to be constrained in the DFT calculations by the ^{131}In magnetic moment.

The results of both ab initio and DFT types of calculation are shown along side the experimental Q and μ moments in Fig. 1a, b, respectively, for the $9/2^+$ states of $^{105-131}$In. The μ moments of the $1/2^-$ states are shown in Fig. 3. All experimental data are presented in Table 1 and Extended Data Table 1, and compared with literature values that exist for $^{105-127}$In.

Results and discussion

In the single-particle picture, a proton-hole configuration induces an intrinsic polarization of the whole nucleus, as indicated schematically in Fig. 1 (bottom left). A gradual decrease in the quadrupole moments of the $9/2^+$ states was previously observed up to $N = 78$. Our measurements show a notably larger decrease at $N = 82$, indicating a marked decrease in polarization (Fig. 1a), as the value expected for the single-proton-hole configuration[36,37] is reached.

The VS-IMSRG calculations reproduce the experimental trends, that is, local variations in neutron number, a dip around $N = 64$ and a gradual decrease towards $N = 82$. However, the magnitude of the Q is underestimated. The reproduction of the magnitude of the quadrupole moments is a known challenge for ab initio nuclear theory, as the Q moments are a highly collective emergent property of the nucleus that can require the inclusion of extensive many-body correlations[38].

Conversely, our DFT calculations are able to closely reproduce the overall magnitude of the Q moments. As $N = 82$ is approached, the agreement with the calculations without pairing (HF) shows that describing individual neutron orbitals becomes important. However, owing to effects induced by occupying individual neutron orbitals, an inaccurate staggering with neutron number is also produced, compared with HFB. As shown in Fig. 1a, time-odd contributions have a negligible effect on Q moments.

In contrast to the Q moments, the μ moments of the $9/2^+$ states were known to exhibit little variation[7], which is continued up to ^{129}In in our observation. However, we observe an abrupt increase at ^{131}In, see Fig. 1b, and the atomic spectra in Extended Data Fig. 1. The extreme single-particle magnetic moment of a proton in the $\pi g_{9/2}$ orbit, the so-called 'Schmidt' limit[39], is also indicated in Fig. 1b.

Our results now show a value much closer to the extreme single-particle limit at $N = 82$, in agreement with decay spectroscopy and moment measurements in the region[40–44]. The μ value at ^{131}In reaches 93% of the Schmidt free-particle value and 81–84% for $N < 82$. However, the sudden change in the μ values from $N < 82$ to $N = 82$ indicates a departure from the single-particle picture for the former, which contradicts the generally accepted conclusions from the earlier magnetic moment[6,7] and transfer reaction[45] studies. Extension of transfer reaction studies to isotopes in the $N = 82$ region would therefore be highly valuable and should be possible in the near future with the development of experiments at radioactive beam facilities, such as SOLARIS at FRIB[46] and ISS at ISOLDE[47].

Owing to the standard angular-momentum coupling rules, the nuclear quadrupole moments can be measured only in states with $I > 1/2$. The $I = 9/2^+$ states of the indium isotopes thus provide access simultaneously to the nuclear quadrupole moments and nuclear magnetic dipole moments. The indium isotopes are therefore a unique case to study the effect of single-proton-hole coupling to the nuclear core on both observables. This is in contrast to thallium ($Z = 81$), the heavier experimentally accessible proton-hole isotopic chain, which has a $1/2^+$ configuration.

Table 1 | The magnetic hyperfine structure parameters, A_{hf}, measured in this work for the odd-mass $^{113-131}$In isotopes and corresponding extracted magnetic dipole moment values.

		A_{hf} (MHz)					
A	I	$5p\ ^2P_{3/2}$	$9s\ ^2S_{1/2}$	$5p\ ^2P_{1/2}$	$8s\ ^2S_{1/2}$	μ^a (μ_N)	$\mu^{Lit.}$ (μ_N)
105	$9/2^+$						+5.675(5)[7]
107	$9/2^+$						+5.585(8)[7]
109	$9/2^+$						+5.538(4)[7]
111	$9/2^+$						+5.503(7)[7]
113	$9/2^+$	+241.8(8)	+130(1)	+2,276.0(8)	+242.7(8)	+5.5264(19)	+5.5289(2)[55]
113	$1/2^-$	−87(10)	−38(20)	−774(50)	−90(50)	−0.21(1)	−0.21074(2)[56]
115	$9/2^+$	+239.9(5)	+130.3(8)	+2,281.9(8)	+243.3(6)	+5.5408(2)[a]	+5.5408(2)[57]
115	$1/2^-$	−96(3)	−48(9)	−903(20)	−66(10)	−0.2405(38)	−0.24398(5)[58]
117	$9/2^+$	+241(4)	+130(5)	+2,277(2)	+244(2)	+5.5286(43)	+5.519(4)[7]
117	$1/2^-$	−106(4)	−49(10)	−1,028(10)	−113(8)	−0.276(27)	−0.25174(3)[7]
119	$9/2^+$	+240(4)	+130(5)			+5.499(62)	+5.515(1)[7]
119	$1/2^-$	−132(7)	−70(10)			−0.342(12)	−0.319(5)[7]
121	$9/2^+$	+243(4)	133(5)			+5.575(62)	+5.502(5)[7]
121	$1/2^-$	−140(2)	−85(6)			−0.3600(41)	−0.355(4)[7]
123	$9/2^+$	+238(4)	+129(5)			+5.442(61)	+5.491(7)[7]
123	$1/2^{(-)}$	−160(2)	−80(5)			−0.4047(54)	−0.400(4)[7]
125	$9/2^+$	+240.3(6)	+129.9(8)			+5.496(24)	+5.502(9)[7]
125	$1/2^{(-)}$	−176(7)	−90(10)			−0.450(17)	−0.433(4)[7]
127	$9/2^+$	+241.8(7)	+130(1)	+2,278.3(6)	+243.8(4)	+5.5321(14)	+5.522(8)[7]
127	$1/2^{(-)}$	−171(3)	−91(10)	−1,613(9)	−174(8)	−0.4355(24)	
129	$(9/2^+)$	+243.3(8)	+132(1)	+2,304.9(9)	+244.8(7)	+5.5961(23)	
129	$1/2^{(-)}$	−156(3)	−80(4)	−1,434(2)	−162(10)	−0.3871(6)	
131	$(9/2^+)$	+275.9(6)	+149.3(7)			+6.312(14)	
131	$1/2^{(-)}$	−20(7)	−11(4)	−188(20)	−20(2)	−0.051(3)	

[a]These μ values were determined using a reference NMR value of μ=+5.5408(2) μ_N (ref. [57]). Lit., literature.

We find that the inclusion of time-odd fields proves to be the primary missing component of the mean field for an accurate description of magnetic moments. We observe that, without the time-odd mean fields, the DFT value obtained for ^{131}In is close to the single-particle value. However, the addition of a spin–spin interaction term corresponding to the isovector Landau parameter[48] of $g'_0 = 0.82$ generates time-odd mean fields that result in a perfect agreement between the DFT and the experimental ^{131}In magnetic moment. The same value of g'_0 was kept in lighter indium isotopes, so the reproduced abrupt change of μ between ^{129}In and ^{131}In was obtained without further adjustment of parameters. The value of g'_0 adopted here is about two standard deviations smaller than that of $g'_0 = 1.7(4)$ obtained in the recent global analysis of ref. [49], which—for other Skyrme functionals—gave values of $g'_0 = 1.3(4)$ and 1.0(4). It is also smaller than that of $g'_0 = 1.2 = 1.2$ recommended in refs. [48,50] based on the analysis of the Gamow–Teller β decays and better aligned with that of $g'_0 = 0.6(1)$ extracted in ref. [51] from the Gamow–Teller response functions; see also discussions in refs. [52,53]. Further studies are needed to see whether the time-odd mean fields can be consistently modelled by the single spin–spin term or a more involved description is needed.

To further investigate the abrupt change that was observed at $N = 82$ within the DFT framework, we traced back the properties of μ in indium directly to those of their polarized cores. To this end, we performed symmetry-restoration HF calculations by filling in the deformed odd-proton holes obtained in the self-consistent DFT states in indium. In this way, we gained access to the corresponding 0^+, 1^+, 2^+, 3^+, 4^+,... states of the polarized tin core. The effect of their contributions to μ in indium is summarized in Fig. 2. The coupling to the 0^+ state of the tin core gives results identical to the Schmidt limit. At this point, it is essential to note that, without the time-odd mean fields, the core is not spin-polarized and, therefore, its states conserve signature symmetry and odd-angular-momentum components vanish. The effect of the time-odd mean fields on magnetic moments thus proceeds through the coupling to the 1^+, 3^+,..., 9^+ states of the polarized core. As shown in Fig. 2, the experimental value in ^{131}In is reproduced by adding only the 1^+ core state to the 0^+. Contributions of higher odd-I states were negligible. For the $N < 82$ isotopes, contributions of the 1^+ core states stay approximately constant. Coupling of the unpaired proton to the even-I polarized core states, which are non-existent at the $N = 82$ shell closure but appear when the neutron shell opens, result in the strong decrease of the magnetic moment when moving away from $N = 82$. Even-I contributions beyond $I^\pi = 6^+$ were negligible. When combined with the 1^+ core polarization contribution, the experimental values are closely reproduced. As the even-I core excitations would also be blocked at the neutron shell closure of $N = 50$, a measurement of the magnetic moment at $N = 50$ would thus show its magicity.

Our results highlight an important difference between the HFB and HF treatments, which is related to the effect of pair breaking. As the neutron pairing vanishes at the shell closure, the calculated magnetic moment of ^{131}In is the same for HF and HFB calculations. For isotopes with $N < 82$, the HF calculations, which include the polarization induced by the broken neutron pairs, reproduce the steep decrease of the magnetic moment, as soon as two holes occur. By contrast, the HFB results, which do not entail broken pairs, do not reproduce that decrease. Further theoretical developments, such as a multi-reference version of HFB to include the mixing of deformed two-quasiparticle excited states, are needed in the HFB framework.

Previously, the decreasing μ values of the $1/2^-$ isomeric states with increasing neutron number (see Fig. 3) were not explained by nuclear theory. Our new experimental results for ^{129,131}In show a sudden increase, which crosses the extreme single-particle value at $N = 82$. The results are compared with literature values of $^{115-127}$In in Table 1. We find that the DFT calculations without pairing correlations also provide a better description than those with pairing correlations (HFB). The introduction of time-odd fields improves the agreement with experiment. However, the pronounced increase at $N = 82$ is not reproduced within this framework, with predictions close to the single-particle limit. Yet, the experimentally observed variation, and crossing of the single-particle limit at $N = 82$, suggests that the $1/2^-$ isomers are sensitive to collectivity. Our VS-IMSRG calculations provide some insight here. Overall, these calculations provide a good description of the previously unexplained trend observed for the magnetic moments of the $1/2^-$ states. Analysis of the VS-IMSRG calculations indicates that the $1/2^-$ state contains a substantial component resulting from the coupling between the $9/2^+$ single-particle configuration and the 5^- (anti-aligned neutrons in the $h_{11/2}$ and $s_{1/2}$ orbitals) state of the core. This therefore suggests that further refinement of the present DFT calculations would be needed to explicitly include other core configurations, for example, negative-parity states, to accurately describe the $1/2^-$ states.

Summary and outlook

The indium isotopes have been considered a textbook example for the dominance of single-particle properties in heavy nuclei. Here we show that their ground-state electromagnetic properties markedly differ at $N = 82$ compared with $N < 82$, despite the single unpaired proton ($\pi g_{9/2}$ proton orbit) dominating the behaviour of this complex many-body system.

Our new experimental results for ^{129,131}In show that, on reaching the neutron-rich magic number $N = 82$, abrupt changes of their electromagnetic properties are observed, and only at the neutron magic number is the single-particle structure almost fully recovered. This challenges our previous understanding of these isotopes, which were assumed to have a single-particle description by invoking the use of empirical effective operators.

We presented two complementary nuclear models to investigate how these seemingly simple structures emerge from the complex interactions among nucleons. Both DFT and ab initio calculations provide a good description of the experimental trends. Within the DFT framework, the intricate isotopic dependence of the indium magnetic and electric ground-state moments turns out to require correct treatment of spin and shape polarization exerted by the proton hole on the $Z = 50$ magic core. The inclusion of time-odd mean fields was shown to be essential to reproduce the experimental findings.

Indium nuclei can coexist in long-lived excited states with $I^\pi = 1/2^-$. The structure of these states was suggested to be dominated by a single unpaired proton in the $\pi p_{1/2}$ orbit. However, in contrast to the simple trends observed for the ground states, the magnetic moments of the $1/2^-$ states exhibit a large variation with neutron number, previously considered a puzzle in the region[7]. These features and the new experimental observations are well described by our ab initio calculations, for which these isotopes in the region of $Z = 50$ are the frontier of such ab initio calculations of nuclear moments[9,10]. Our work indicates a very mixed configuration for the isomeric states, which is not yet captured with the DFT calculations, in which negative parity core polarization needs to be included.

Although our ab initio calculations provide a good description of the experimental trends, they fall short in reproducing the magnitude of the $9/2^+$ electromagnetic moments. This may be attributed to the lack of inclusion of many-body currents, which are known to be essential to describe the electromagnetic properties of light nuclei[54]. Future theoretical developments would be needed to include many-body currents and clarify the role that they play in heavy nuclei. On the other hand, a theoretical description of the nuclear quadrupole moments requires the extensive inclusion of neglected many-body correlations. Thus, our new experimental results at $N = 82$ provide critical data for future developments of both ab initio and DFT theory.

Our experimental results for ^{131}In allowed an investigation of the strength of the time-odd mean fields, which—until now—have been poorly constrained in DFT theories. Such time-odd channels are essential for a correct description of numerous nuclear properties, such as double-beta-decay rates[34], permanent electric dipole moment measurements[32,33] and dark matter searches[35]. This provides strong motivation to extend experiments to other isotopes possessing single-hole (particle) with respect to suggested nuclear closed shells at extreme proton-to-neutron ratios. In addition, further theoretical developments are needed to investigate the role of meson-exchange currents and further non-nucleonic degrees of freedom in nuclear moments.

Online content

Any methods, additional references, Nature Research reporting summaries, source data, extended data, supplementary information, acknowledgements, peer review information; details of author contributions and competing interests; and statements of data and code availability are available at https://doi.org/10.1038/s41586-022-04818-7.

1. Schmidt, T. The electric quadrupole moment of the nucleus. *Nature* **138**, 404 (1936).
2. Jones, K. L. et al. The magic nature of ^{132}Sn explored through the single-particle states of ^{133}Sn. *Nature* **465**, 454–457 (2010).
3. Taniuchi, R. et al. ^{78}Ni revealed as a doubly magic stronghold against nuclear deformation. *Nature* **569**, 53–58 (2019).
4. Togashi, T., Tsunoda, Y., Otsuka, T., Shimizu, N. & Honma, M. Novel shape evolution in Sn isotopes from magic numbers 50 to 82. *Phys. Rev. Lett.* **121**, 062501 (2018).
5. Jenkins, D. G. Recent advances in nuclear physics through on-line isotope separation. *Nat. Phys.* **10**, 909–913 (2014).
6. Heyde, K. L. G. *The Nuclear Shell Model. Springer Series in Nuclear and Particle Physics* (Springer, 1990).
7. Eberz, J. et al. Spins, moments and mean square charge radii of $^{104-127}$In determined by laser spectroscopy. *Nucl. Phys. A* **464**, 9–28 (1987).
8. Rosiak, D. et al. Enhanced quadrupole and octupole strength in doubly magic ^{132}Sn. *Phys. Rev. Lett.* **121**, 252501 (2018).
9. Gysbers, P. et al. Discrepancy between experimental and theoretical β-decay rates resolved from first principles. *Nat. Phys.* **15**, 428–431 (2019).
10. Morris, T. D. et al. Structure of the lightest tin isotopes. *Phys. Rev. Lett.* **120**, 152503 (2018).
11. Schunck, N. (ed.) *Energy Density Functional Methods for Atomic Nuclei* 2053–2563 (IOP Publishing, 2019).
12. Rodríguez, L. V. et al. Doubly-magic character of ^{132}Sn studied via electromagnetic moments of ^{133}Sn. *Phys. Rev. C* **102**, 051301 (2020).
13. Hinke, C. B. et al. Superallowed Gamow–Teller decay of the doubly magic nucleus ^{100}Sn. *Nature* **486**, 341–345 (2012).
14. Manea, V. et al. First glimpse of the $N = 82$ shell closure below $Z = 50$ from masses of neutron-rich cadmium isotopes and isomers. *Phys. Rev. Lett.* **124**, 092502 (2020).
15. Neyens, G. Nuclear magnetic and quadrupole moments for nuclear structure research on exotic nuclei. *Rep. Prog. Phys.* **66**, 633–689 (2003).
16. Stroberg, S. R., Bogner, S. K., Hergert, H. & Holt, J. D. Nonempirical interactions for the nuclear shell model: an update. *Annu. Rev. Nucl. Part. Sci.* **69**, 307–362 (2019).
17. Hebeler, K., Bogner, S. K., Furnstahl, R. J., Nogga, A. & Schwenk, A. Improved nuclear matter calculations from chiral low-momentum interactions. *Phys. Rev. C* **83**, 031301 (2011).
18. de Groote, R. et al. Precision measurement of the magnetic octupole moment in ^{45}Sc as a test for state-of-the-art atomic-and nuclear-structure theory. *Phys. Lett. B* **827**, 136930 (2022).
19. Bennaceur, K., Dobaczewski, J., Haverinen, T. & Kortelainen, M. Properties of spherical and deformed nuclei using regularized pseudopotentials in nuclear DFT. *J. Phys. G Nucl. Part. Phys.* **47**, 105101 (2020).
20. Dobaczewski, J. et al. Mean-field description of ground-state properties of drip-line nuclei: pairing and continuum effects. *Phys. Rev. C* **53**, 2809–2840 (1996).
21. Dobaczewski, J., Flocard, H. & Treiner, J. Hartree-Fock-Bogolyubov description of nuclei near the neutron-drip line. *Nucl. Phys. A* **422**, 103–139 (1984).
22. Sheikh, J. A., Dobaczewski, J., Ring, P., Robledo, L. M. & Yannouleas, C. Symmetry restoration in mean-field approaches. *J. Phys. G Nucl. Part. Phys.* **48**, 123001 (2021).
23. Cocolios, T. E. et al. High-resolution laser spectroscopy with the Collinear Resonance Ionisation Spectroscopy (CRIS) experiment at CERN-ISOLDE. *Nucl. Instrum. Methods Phys. Res. B Beam Interact. Mater. Atoms* **376**, 284–287 (2016).
24. Sahoo, B. K. et al. Analytic response relativistic coupled-cluster theory: the first application to indium isotope shifts. *New J. Phys.* **22**, 012001 (2020).
25. Vernon, A. et al. Simulation of the relative atomic populations of elements 1<=*Z*<=89 following charge exchange tested with collinear resonance ionization spectroscopy of indium. *Spectrochim. Acta Part B At. Spectrosc.* **153**, 61–83 (2019).

26. Garcia Ruiz, R. F. et al. High-precision multiphoton ionization of accelerated laser-ablated species. *Phys. Rev. X* **8**, 041005 (2018).
27. Epelbaum, E., Hammer, H.-W. & Meißner, U.-G. Modern theory of nuclear forces. *Rev. Mod. Phys.* **81**, 1773–1825 (2009).
28. Machleidt, R. & Entem, D. R. Chiral effective field theory and nuclear forces. *Phys. Rep.* **503**, 1–75 (2011).
29. Jiang, W. G. et al. Accurate bulk properties of nuclei from $A = 2$ to ∞ from potentials with Δ isobars. *Phys. Rev. C* **102**, 054301 (2020).
30. Engel, Y., Brink, D., Goeke, K., Krieger, S. & Vautherin, D. Time-dependent Hartree-Fock theory with Skyrme's interaction. *Nucl. Phys. A* **249**, 215–238 (1975).
31. Perlińska, E., Rohoziński, S. G., Dobaczewski, J. & Nazarewicz, W. Local density approximation for proton-neutron pairing correlations: formalism. *Phys. Rev. C* **69**, 014316 (2004).
32. Dobaczewski, J., Engel, J., Kortelainen, M. & Becker, P. Correlating Schiff moments in the light actinides with octupole moments. *Phys. Rev. Lett.* **121**, 232501 (2018).
33. Chupp, T. E., Fierlinger, P., Ramsey-Musolf, M. J. & Singh, J. T. Electric dipole moments of atoms, molecules, nuclei, and particles. *Rev. Mod. Phys.* **91**, 015001 (2019).
34. Dolinski, M. J., Poon, A. W. & Rodejohann, W. Neutrinoless double-beta decay: status and prospects. *Annu. Rev. Nucl. Part. Sci.* **69**, 219–251 (2019).
35. Engel, J., Pittel, S. & Vogel, P. Nuclear physics of dark matter detection. *Int. J. Mod. Phys. E* **1**, 1–37 (1992).
36. Co', G., Donno, V. D., Anguiano, M., Bernard, R. N. & Lallena, A. M. Electric quadrupole and magnetic dipole moments of odd nuclei near the magic ones in a self-consistent approach. *Phys. Rev. C* **92**, 024314 (2015).
37. Krane, K. S. & Halliday, D. *Introductory Nuclear Physics* (Wiley, 1988).
38. Henderson, J. et al. Testing microscopically derived descriptions of nuclear collectivity: Coulomb excitation of ^{22}Mg. *Phys. Lett. B* **782**, 468–473 (2018).
39. Schmidt, T. Über die magnetischen Momente der Atomkerne. *Z. Phys.* **106**, 358–361 (1937).
40. Taprogge, J. et al. $^{1}p_{3/2}$ proton-hole state in ^{132}Sn and the shell structure along $N = 82$. *Phys. Rev. Lett.* **112**, 132501 (2014).
41. Fogelberg, B. et al. Decays of ^{131}In, ^{131}Sn, and the position of the $h_{11/2}$ neutron hole state. *Phys. Rev. C* **70**, 034312 (2004).
42. Fogelberg, B. & Blomqvist, J. Single-hole and three-quasiparticle levels in ^{131}Sn observed in the decay of ^{131g,m1,m2}In. *Nucl. Phys. A* **429**, 205–217 (1984).
43. Vaquero, V. et al. Fragmentation of single-particle strength around the doubly magic nucleus ^{132}Sn and the position of the $^{0}f_{5/2}$ proton-hole state in ^{131}In. *Phys. Rev. Lett.* **124**, 022501 (2020).
44. Lechner, S. et al. Probing the single-particle behavior above ^{132}Sn via electromagnetic moments of ^{133,134}Sb and $n = 82$ isotones. *Phys. Rev. C* **104**, 014302 (2021).
45. Weiffenbach, C. V. & Tickle, R. Structure of odd-*a* indium isotopes determined by the (d, ^{3}He) reaction. *Phys. Rev. C* **3**, 1668–1678 (1971).
46. Kay, B. The SOLARIS spectrometer. In *APS April Meeting Abstracts* Q13.002 (APS, 2019).
47. Tang, T. L. et al. First exploration of neutron shell structure below lead and beyond $n = 126$. *Phys. Rev. Lett.* **124**, 062502 (2020).
48. Bender, M., Dobaczewski, J., Engel, J. & Nazarewicz, W. Gamow-Teller strength and the spin-isospin coupling constants of the Skyrme energy functional. *Phys. Rev. C* **65**, 054322 (2002).
49. Sassarini, P. L., Dobaczewski, J., Bonnard, J. & Garcia Ruiz, R. F. Global analysis of electromagnetic moments in odd near doubly magic nuclei. Preprint at https://arxiv.org/abs/2111.04675 (2021).
50. Borzov, I. N., Tolokonnikov, S. V. & Fayans, S. Spin-dependent effective nucleon-nucleon interaction in nuclei. *Sov. J. Nucl. Phys.* **40**, 732–739 (1984).
51. Wakasa, T., Ichimura, M. & Sakai, H. Unified analysis of spin isospin responses of nuclei. *Phys. Rev. C* **72**, 067303 (2005).
52. Roca-Maza, X., Colò, G. & Sagawa, H. New Skyrme interaction with improved spin-isospin properties. *Phys. Rev. C* **86**, 031306 (2012).
53. Davesne, D., Pastore, A. & Navarro, J. Linear response theory with finite-range interactions. *Prog. Part. Nucl. Phys.* **120**, 103870 (2021).
54. Pastore, S., Pieper, S. C., Schiavilla, R. & Wiringa, R. B. Quantum Monte Carlo calculations of electromagnetic moments and transitions in $A \leq 9$ nuclei with meson-exchange currents derived from chiral effective field theory. *Phys. Rev. C* **87**, 035503 (2013).
55. Rice, M. & Pound, R. V. Ratio of the magnetic moments of In^{115} and In^{113}. *Phys. Rev.* **106**, 953–953 (1957).
56. Childs, W. J. & Goodman, L. S. Nuclear spin and hyper-fine Interaction of In^{113m}. *Phys. Rev.* **118**, 1578–1581 (1960).
57. Flynn, C. P. & Seymour, E. F. W. Knight shift of the nuclear magnetic resonance in liquid indium. *Proc. Phys. Soc.* **76**, 301–303 (1960).
58. Cameron, J. A., King, H. J., Eastwood, H. K. & Summers-Gill, R. G. The magnetic moment of indium-115*m*. *Can. J. Phys.* **40**, 931–942 (1962).

Methods

The collinear resonance ionization setup

The indium isotopes were produced at CERN's online isotope separator facility, ISOLDE, by impinging 1.4-GeV protons onto the proton-to-neutron converter of a thick uranium-carbide target[59]. The converter suppressed nearby caesium mass contamination[60]. The indium isotopes diffused through the target material and their ionization was greatly enhanced by the use of the resonance laser ion source, RILIS[61]. The produced indium ions were then accelerated to 40 keV and mass separated using the ISOLDE high-resolution mass separator before being cooled and bunched using a gas-filled linear Paul trap (ISCOOL)[62,63]. After a trapping time of up to 10 ms, ion bunches with a temporal width of 2 μs were then re-accelerated to 40,034(1) eV and deflected into the CRIS beamline[23,64]. The indium ions were then neutralized with a sodium-filled charge-exchange cell with an efficiency of up to 60% and predicted relative atomic populations of 57% and 37%, respectively, for the $5p\ ^2P_{3/2}$ metastable state and the $5p\ ^2P_{1/2}$ ground state[65]. The remaining ion fraction was removed by electrostatic deflectors, and the neutralized atom bunch was collinearly overlapped with two pulsed lasers, one for excitation and another for non-resonant ionization. The atoms were resonantly excited using two different ultraviolet transitions in separate measurements, the first using 246.8-nm laser light for the $5p\ ^2P_{3/2} \rightarrow 9s\ ^2S_{1/2}$ atomic transition and the second using 246.0-nm laser light for the $5p\ ^2P_{1/2} \rightarrow 8s\ ^2S_{1/2}$ atomic transition, which is more sensitive to nuclear magnetic moments, μ, but alone does not give the nuclear electric quadrupole moment, Q. The resonant laser light was produced by frequency tripling the light from an injection-locked Ti:sapphire laser system[66]. This laser was seeded using a narrowband SolsTiS continuous-wave Ti:sapphire laser and pumped using a Lee Laser LDP-100MQ Nd:YAG laser, producing pulsed narrowband 740(738)-nm laser light at 1-kHz repetition rate. This light was then frequency tripled to 246.8(246.0)-nm light by the use of two non-linear crystals[67]. About 3 μJ of laser light was used to saturate both transitions. The excited atoms were then ionized by a final non-resonant 1,064-nm step, provided by a Litron LPY 601 50–100 PIV Nd:YAG laser at 100-Hz repetition rate. The frequency of the resonant first step was scanned and the resulting ions were deflected onto a detector, producing the hyperfine structure containing spectra from which the hyperfine parameters were obtained. The wavelengths were measured using a HighFinesse WSU-2 wavelength meter, which was drift stabilized by simultaneous measurement of a TOPTICA DLC DL Pro 780 diode laser locked to the $5s\ ^2S_{1/2} \rightarrow 5p\ ^2P_{3/2}$ F = 2 → 3 transition of ^{87}Rb using a saturated absorption spectroscopy unit.

Evaluation of nuclear magnetic and quadrupole moments

The μ values were determined using a reference NMR value of $\mu_{ref} = +5.5408(2)\ \mu_N$ for ^{115}In (ref. [57]) and the relation

$$\mu = \mu_{ref} \frac{IA}{I_{ref}, A_{ref}} (1 + \Delta), \quad (1)$$

in which the differential hyperfine anomaly, Δ, is negligible for these atomic states of indium[68]. Here A_{ref} are our experimentally determined values for the $5p^2\ P_{3/2}$, $9s^2\ S_{1/2}$, $5p^2\ P_{1/2}$ and $8s^2\ S_{1/2}$ states of stable ^{115}In and A are those of short-lived isotopes. The final μ values presented in Table 1 are a weighted average of the μ values from each atomic state, which were self-consistent within 2σ.

The spectroscopic nuclear electric quadrupole moments, Q, were extracted using the relation

$$B_{hf} = e\ Q\ V_{ZZ}\ , \quad (2)$$

in which a value of $B_{hf}(^2P_{3/2})/Q = 576(4)$ MHz/b was used, obtained from relativistic coupled-cluster atomic calculations[26]. Here V_{ZZ} is the electric field gradient produced by the electrons at the nucleus.

The ratio of A_{hf} factors depends dominantly on atomic structure and therefore remains constant when the correct nuclear spin assignment is used for fitting of spectra resulting from hyperfine structure[69]. Although reduced χ^2 fitting of the spectra (as shown in Extended Data Fig. 1) resulted in minima when we use $I = 9/2$, the spin assignment from the ratio of upper and lower atomic state A_{hf} factors (of the $5p\ ^2P_{3/2} \rightarrow 9s\ ^2S_{1/2}$ transition) could not rule out nuclear spins 7/2 and 11/2 outside 1σ uncertainty. The spin of the $I = 9/2$ states are tentatively assigned by experiment and strongly supported by nuclear theory. The spin assignments of the $I = 1/2$ states were confirmed unambiguously from the number of peaks in their spectra.

VS-IMSRG calculations

The VS-IMSRG calculations start from the underlying NN and 3N interactions expressed in the harmonic-oscillator basis. We then construct an effective Hamiltonian designed for a particular valence space in which the exact diagonalization is feasible[16]. The effective Hamiltonian was decoupled from the full A-body Hamiltonian through the application of an approximate unitary transformation derived from the Magnus expansion method[70]. Using the same transformation, the effective $M1$ and $E2$ valence-space operators were then decoupled consistently with the Hamiltonian. During the calculation, all of the operators arising in nested commutator expansions were truncated at the two-body level, the IMSRG(2) approximation.

We begin in a spherical-harmonic-oscillator basis with a frequency of $\hbar\omega = 16$ MeV and $e = 2n + l \leq e_{max} = 14$ for 1.8/2.0(EM)[17,71] (and 12 for N^2LO_{GO}), with a further cut of $e_1 + e_2 + e_3 \leq E_{3max} = 16$ imposed owing to storage limitations of 3N matrix elements. The valence space was taken as the proton $\{1p_{1/2}, 1p_{3/2}, 0f_{5/2}, 0g_{9/2}\}$ and neutron $\{2s_{1/2}, 1d_{3/2}, 1d_{5/2}, 0g_{7/2}, 0h_{11/2}\}$ single-particle orbits above the ^{78}Ni core.

To investigate the effect of valence space on the calculations, the calculations were also performed with the proton $\{1p_{1/2}, 1p_{3/2}, 0f_{5/2}, 0g_{9/2}\}$ and neutron $\{2s_{1/2}, 1d_{3/2}, 0h_{11/2}, 1f_{7/2}\}$ valence space above the ^{92}Ni core. Values of the $9/2^+$ states varied by <2% and $1/2^-$ by <25%, owing to the increased sensitivity of the 1/2 states to collectivity. The trends over neutron number in the calculations obtained were unaffected. The final valence-space diagonalization and evaluation of electromagnetic moments were performed with the KSHELL code[72]. The effect of fully accounting for translation invariance in the $M1$ operator was found to be less than 1%, largely owing to the lack of radial dependence of the $M1$ operator.

DFT calculations

We performed the DFT calculations using code HFODD[73,74] version (3.01m) and a standard Skyrme density functional UNEDF1 (ref. [75]). The deformed DFT single-particle wave functions were expanded on the spherical-harmonic-oscillator basis up to $N_0 = 16$ quanta. An A-dependent harmonic-oscillator frequency $\hbar\omega$ was fixed according to the prescription defined in ref. [76]. For the state $9/2^+$, the proton configuration (with no pairing correlations) was fixed by occupying 49 lowest axially deformed prolate orbitals, that is, the Nilsson orbital $[404]\frac{9}{2}$ with the angular-momentum projection on the symmetry axis $\Omega = -9/2$ was left empty. Similarly, for the state $1/2^-$, the hole was kept in the oblate Nilsson orbital $[301]\frac{1}{2}$ with $\Omega = -1/2$. It was essential to pick the proton-hole configurations with angular momenta properly aligned along the axial-symmetry axis. Indeed, as discussed in refs. [77,78], the time-odd mean fields and core spin-polarization depend on the relative orientation of the intrinsic angular momentum and shape.

For both proton configurations, the open-shell neutron configurations were constructed either with (HFB results) or without (HF results) pairing correlations included. For all deformed mean-field states $|\Omega\rangle$ obtained in this way, which were eigenstates of the z-component of the angular momentum, $\hat{I}_z|\Omega\rangle = \Omega|\Omega\rangle$, we performed the total angular-momentum restoration[22] by evaluating the integral

$$|IM\rangle = N_{IM}\int_{\beta=0}^{\pi} \mathrm{d}\beta\, d^{I}_{M\Omega}(\beta)\exp(-\mathrm{i}\beta\hat{I}_{y})|\Omega\rangle, \quad (3)$$

in which $d^{I}_{M\Omega}(\beta)$ are the Wigner functions[79], M is the projection of the angular momentum on the laboratory z-axis and N_{IM} is a normalization factor. This allowed us to determine the standard spectroscopic magnetic dipole μ and electric quadrupole Q moments[80] as

$$\mu = \sqrt{\frac{4\pi}{3}}\langle II|\hat{M}_{10}|II\rangle \quad \text{and} \quad Q = \sqrt{\frac{16\pi}{5}}\langle II|\hat{Q}_{20}|II\rangle, \quad (4)$$

in which $\hat{M}$ and $\hat{Q}$ are the corresponding $M1$ and $E2$ electromagnetic operators, respectively. In addition, for paired configurations, the particle-number symmetry was restored in a similar way[22]. Neither effective charges nor effective g-factors were used in the ab initio or DFT calculations.

Data availability

Examples of spectra source data for the previously unmeasured ^{129,131}In isotopes, most relevant to this work, are included in this article. The full datasets generated and/or analysed during the current study are available in the Zenodo repository, https://doi.org/10.5281/zenodo.6406949. The code used to analyse the data is also included in the repository.

The data files related to the DFT calculations are available at https://webfiles.york.ac.uk/HFODD/Projects/Magnetic_and_electric_moments_in_Indium/.

Code availability

The code used to analyse the data is included in the Zenodo repository, https://doi.org/10.5281/zenodo.6406949.

The code used to perform the DFT calculations is available at https://webfiles.york.ac.uk/HFODD/Projects/hf301m/.

59. Köster, U. Intense radioactive-ion beams produced with the ISOL method. *Eur. Phys. J. A* **15**, 255–263 (2002).
60. Dillmann, I. et al. Selective laser ionization of N>=82 indium isotopes: the new r-process nuclide ^{135}In. *Eur. Phys. J. A* **13**, 281–284 (2002).
61. Rothe, S., Marsh, B. A., Mattolat, C., Fedosseev, V. N. & Wendt, K. A complementary laser system for ISOLDE RILIS. *J. Phys. Conf. Ser.* **312**, 052020 (2011).
62. Mané, E. et al. An ion cooler-buncher for high-sensitivity collinear laser spectroscopy at ISOLDE. *Eur. Phys. J. A* **42**, 503–507 (2009).
63. Frånberg, H. et al. Off-line commissioning of the ISOLDE cooler. *Nucl. Instrum. Methods Phys. Res. B Beam Interact. Mater. Atoms* **266**, 4502–4504 (2008).
64. Vernon, A. R. et al. Optimising the collinear resonance ionisation spectroscopy (CRIS) experiment at CERN-ISOLDE. *Nucl. Instrum. Methods Phys. Res. B Beam Interact. Mater. Atoms* **463**, 384–389 (2020).
65. Vernon, A. et al. Simulation of the relative atomic populations of elements $1 \le Z \le 89$ following charge exchange tested with collinear resonance ionization spectroscopy of indium. *Spectrochim. Acta Part B At. Spectrosc.* **153**, 61–83 (2019).
66. Sonnenschein, V. et al. Characterization of a pulsed injection-locked Ti:sapphire laser and its application to high resolution resonance ionization spectroscopy of copper. *Laser Phys.* **27**, 085701 (2017).
67. Bass, M., Franken, P. A., Hill, A. E., Peters, C. W. & Weinreich, G. Optical mixing. *Phys. Rev. Lett.* **8**, 18 (1962).
68. Persson, J. R. Table of hyperfine anomaly in atomic systems. *At. Data Nucl. Data Tables* **99**, 62–68 (2013).
69. Cheal, B. et al. Nuclear spins and moments of Ga isotopes reveal sudden structural changes between $N = 40$ and $N = 50$. *Phys. Rev. Lett.* **104**, 252502 (2010).
70. Morris, T. D., Parzuchowski, N. M. & Bogner, S. K. Magnus expansion and in-medium similarity renormalization group. *Phys. Rev. C* **92**, 34331 (2015).
71. Simonis, J., Stroberg, S. R., Hebeler, K., Holt, J. D. & Schwenk, A. Saturation with chiral interactions and consequences for finite nuclei. *Phys. Rev. C* **96**, 014303 (2017).
72. Shimizu, N., Mizusaki, T., Utsuno, Y. & Tsunoda, Y. Thick-restart block Lanczos method for large-scale shell-model calculations. *Comput. Phys. Commun.* **244**, 372–384 (2019).
73. Schunck, N. et al. Solution of the Skyrme-Hartree–Fock–Bogolyubov equations in the Cartesian deformed harmonic-oscillator basis. (VIII) HFODD (v2.73y): a new version of the program. *Comput. Phys. Commun.* **216**, 145–174 (2017).
74. Dobaczewski, J. et al. Solution of universal nonrelativistic nuclear DFT equations in the Cartesian deformed harmonic-oscillator basis. (IX) HFODD (v3.06h): a new version of the program. *J. Phys. G Nucl. Part. Phys.* **48**, 102001 (2021).
75. Kortelainen, M. et al. Nuclear energy density optimization: large deformations. *Phys. Rev. C* **85**, 024304 (2012).
76. Dobaczewski, J. & Dudek, J. Solution of the Skyrme–Hartree–Fock equations in the Cartesian deformed harmonic oscillator basis II. The program HFODD. *Comput. Phys. Commun.* **102**, 183–209 (1997).
77. Schunck, N. et al. One-quasiparticle states in the nuclear energy density functional theory. *Phys. Rev. C* **81**, 024316 (2010).
78. Satuła, W., Bączyk, P., Dobaczewski, J. & Konieczka, M. No-core configuration-interaction model for the isospin- and angular-momentum-projected states. *Phys. Rev. C* **94**, 024306 (2016).
79. Varshalovich, D., Moskalev, A. & Khersonskii, V. *Quantum Theory of Angular Momentum* (World Scientific, 1988).
80. Ring, P. & Schuck, P. *The Nuclear Many-body Problem* (Springer, 1980).

Acknowledgements This work was supported by ERC Consolidator Grant no. 648381 (FNPMLS); STFC grants ST/L005794/1, ST/L005786/1, ST/P004423/1, ST/M006433/1 and ST/P003885/1, and Ernest Rutherford grant no. ST/L002868/1; the U.S. Department of Energy, Office of Science, Office of Nuclear Physics under grant DE-SC0021176; GOA 15/010 from KU Leuven, BriX Research Program No. P7/12; the FWO-Vlaanderen (Belgium); the European Unions Grant Agreement 654002 (ENSAR2); National Key R&D Program of China (contract no. 2018YFA0404403); the National Natural Science Foundation of China (no. 11875073); the Polish National Science Centre under contract no. 2018/31/B/ST2/02220. TRIUMF receives funding by a contribution through the National Research Council of Canada. The theoretical work was further supported by NSERC and the U.S. Department of Energy under contract DE-FG02-97ER41014. The VS-IMSRG computations were performed with an allocation of computing resources on Cedar at WestGrid and Compute Canada, and on the Oak Cluster at TRIUMF managed by the University of British Columbia department of Advanced Research Computing (ARC). We would also like to thank the ISOLDE technical group for their support and assistance and the University of Jyväskylä for the use of the injection-locked cavity. We acknowledge the CSC – IT Center for Science Ltd., Finland, for the allocation of computational resources. This project was partly undertaken on the Viking Cluster, which is a high-performance computing facility provided by the University of York. We are grateful for computational support from the University of York High Performance Computing service, Viking and the Research Computing team.

Author contributions A.R.V. prepared the manuscript with input from all authors, especially R.F.G.R., J.Bo., J.D., J.D.H., T.M., G.N., K.T.F., T.E.C., R.P.deG. and S.R.S. R.F.G.R., J.Bi., C.L.B., M.L.B., T.E.C., K.T.F., W.G., R.P.deG., A.K., K.M.L., G.N., S.G.W., A.R.V. and X.F.Y. proposed the experiment(s), A.R.V., C.L.B., M.L.B., T.E.C., K.T.F., G.J.F.-S., G.G., W.G., R.P.deG., R.H., A.K., D.L., K.M.L., R.F.G.R., S.G.W., X.F.Y. and D.Y. conducted the experiment(s), A.R.V., C.L.B., R.F.G.R. and J.H. analysed the results, J.Bo. and J.D. performed theoretical (DFT) nuclear calculations, J.D.H., T.M. and S.R.S. performed theoretical (VS-IMSRG) nuclear calculations. All authors reviewed the manuscript.

Competing interests The authors declare no competing interests.

Additional information

Supplementary information The online version contains supplementary material available at https://doi.org/10.1038/s41586-022-04818-7.

Correspondence and requests for materials should be addressed to A. R. Vernon or R. F. Garcia Ruiz.

Peer review information *Nature* thanks Gianluca Colo and the other, anonymous, reviewer(s) for their contribution to the peer review of this work.

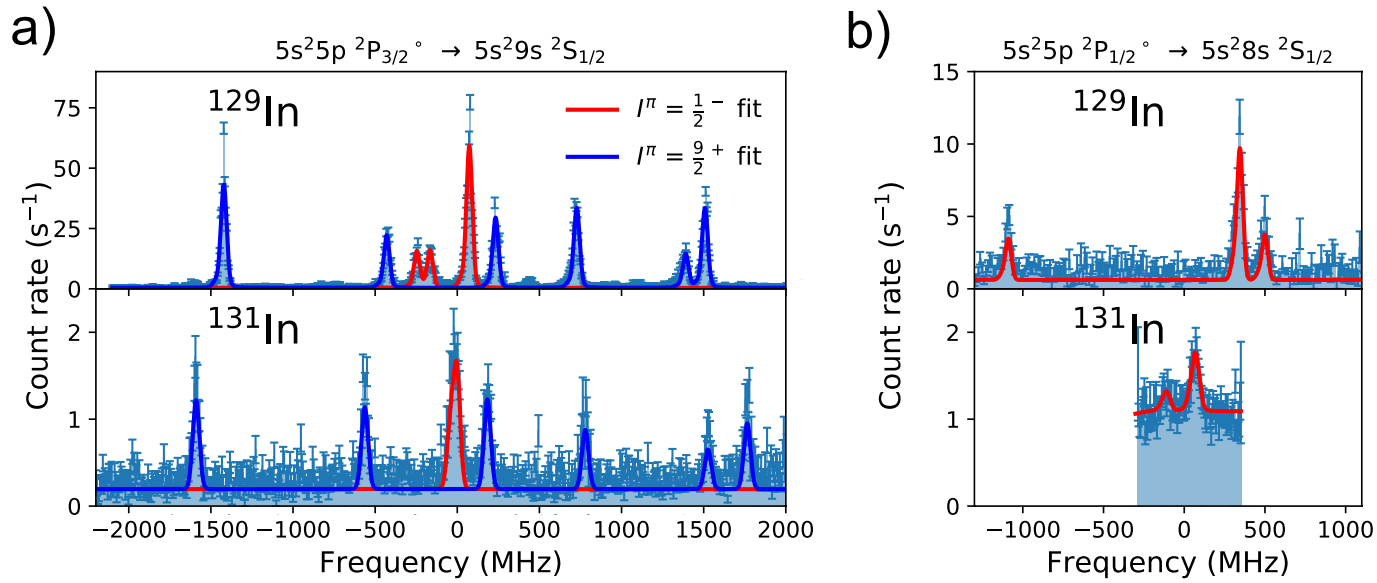

Extended Data Fig. 1 | Example hyperfine spectra of the ^{129}In and ^{131}In isotopes. a, **b**, Example spectra measured using the 246.8-nm ($5p\ ^2P_{3/2} \rightarrow 9s\ ^2S_{1/2}$) transition (**a**), and using the 246.0-nm ($5p\ ^2P_{1/2} \rightarrow 8s\ ^2S_{1/2}$) transition (**b**). The $9/2^+$ ground and $1/2^-$ isomer states are indicated.

Extended Data Table 1 | The B_{hf} hyperfine structure parameter (from the $^2P_{3/2}$ state) values, measured in this work for the odd-mass $^{113-131}$In isotopes and the extracted electric quadrupole moment values

A	I	B_{hf} (MHz)	$Q^{\dagger}$ (eb)	$Q^{Lit.}$ (eb)
105	$9/2^+$			+0.79(5)[15,16]
107	$9/2^+$			+0.77(5)[15,16]
109	$9/2^+$			+0.80(3)[15,16]
111	$9/2^+$			+0.76(2)[15,16]
113	$9/2^+$	+441(15)	+0.767(27)	+0.759(8)[15,16]
115	$9/2^+$	+454.2(65)	+0.789(13)	+0.770(8)[15,16]
117	$9/2^+$	+465(13)	+0.807(23)	+0.788(10)[15,16]
119	$9/2^+$	+462(13)	+0.802(23)	+0.812(7)[15,16]
121	$9/2^+$	+462(13)	+0.803(23)	+0.774(10)[15,16]
123	$9/2^+$	+424(13)	+0.736(23)	+0.720(9)[15,16]
125	$9/2^+$	+382.3(55)	+0.664(11)	+0.68(3)[15,16]
127	$9/2^+$	+338(16)	+0.588(29)	+0.56(3)[15,16]
129	$(9/2^+)$	+280.4(73)	+0.487(13)	
131	$(9/2^+)$	+177.3(57)	+0.310(10)	

† Extracted using a value of $B_{hf}(^2P_{3/2})/Q = +576(4)$ MHz/b[13].